J. Min. Metall. Sect. B-Metall. 58 (3) (2022) 417 - 426

Journal of Mining and Metallurgy, Section B: Metallurgy

CARBOTHERMAL REDUCTION OF FAYALITE: THERMODYNAMIC AND NON-ISOTHERMAL KINETIC ANALYSIS

Z. Li [a, b], G.-J. Ma [a, b, *], J.-J. Zou [a, b], D.-L, Zheng [a, b], X. Zhang [a, b]

[a] The State Key Laboratory of Refractories and Metallurgy, Wuhan University of Science and Technology, Wuhan, China

[b] Key Laboratory for Ferrous Metallurgy and Resources Utilization of Ministry of Education, Wuhan University of Science and Technology, Wuhan, China

(Received 23 March 2021; accepted 26 August 2022)

Abstract

The present paper investigated the thermodynamics and kinetics of carbothermal reduction of fayalite by non-isothermal method combining with thermogravimetric analyzer and applying the Flynn-Wall-Ozawa (FWO) and Málek models. According to the thermodynamic analysis, the starting temperature of direct reduction reaction of fayalite was 806.79 ℃ in the standard state. The indirect reduction reaction could not take place in the standard state. While the volume percentage of CO was higher than 86 vol.% in nonstandard state, the indirect reduction could take place in the range of experimental temperature. Meanwhile, Boudouard reaction could promote the indirect reduction process. The kinetic analysis results showed that at the temperature below 1100 ℃, the main reduction reaction was the direct reduction between fayalite and graphite. With the temperature increasing, the fayalite reacted with CO generated from the gasification of graphite. When the reduction rate increased from 0% to 50%, the activation energy of the reaction increased to 524.41 kJ/mol. Then, the activation energy decreased with the increase of reduction rate. The carbothermal reduction of fayalite was a multistep reaction. The controlling step in the initial stage was the gasification of graphite. As the reaction proceeded, the generated CO provided a good kinetics condition for the carbothermal reduction of fayalite, and the controlling step of the reaction was the nucleation and growth of the metallic iron.

Keywords: *Carbothermal reduction of fayalite; Thermodynamics; Non-isothermal kinetics*

1. Introduction

Copper is widely used in daily life and professional fields. The total world production of refined copper reached 23.9 million tons in 2018 [1]. In China, more than 80% of copper is produced from the copper ores through the pyrometallurgical route, where the copper slag is produced as a kind of by-products [2]. Typically, about 2.2~3.0 tons of copper slag are generated per ton matte produced [3]. Dumping and disposal are the traditional options to treat copper slag, which not only occupies a large amount of land, but also causes serious pollution. Nowadays, copper slag can be used as a raw material for building materials such as cement, concrete, glass and ceramic tiles, as well as grinding and paving materials due to its excellent physical and mechanical properties and good cost-effectiveness [4-6]. However, there are about 30~40 wt% of Fe and 0.5~2.1 wt% of Cu in the copper slag, which are close to or even higher than the corresponding iron or copper ores, respectively [7, 8]. Therefore, rational use of secondary metal resources of copper slag, especially iron resource, is also an important index for comprehensive recovery and utilization of copper slag.

Based on the shortage of high-grade iron ore resources in recent years [9], there are mainly three methods being put forward to extract iron from copper slag, i.e., beneficiation, oxidation-magnetic separation, and carbothermal reduction process. Han et al. [10] utilized the grinding and beneficiation method to explore the recovery of Fe from copper slag, where the iron grade and iron recovery ratio were 54.76% and 65.81%, respectively. Since most of iron in copper slag exists in the form of fayalite (Fe_2SiO_4), which is stable, it coexists with gangues and has weak magnetism, it is hard to get high grades of iron-bearing concentrate by beneficiation process. In recent years, oxidized modification and magnetic separation of copper slag have been developed for improving the iron grade of concentrate obtained from

* *Corresponding author: gma@wust.edu.cn*

https://doi.org/10.2298/JMMB210323022L

copper slag. Researchers oxidized the iron-bearing components in copper slag to magnetite in air or oxidizing atmosphere and then recycled by magnetic separation [11-13]. Jiang et al. [11] recovered iron from copper slag via modified roasting and magnetic separation, and the whole system was in a weak oxidizing atmosphere for the stable equilibrium of CO_2-CO. The iron grade and iron recovery ratio of the obtained iron concentrate were 54.79% and 80.14%, respectively. The iron grade by adopting this method is often low due to the fact that the melting point and viscosity of the slag at the late stage of oxidation reaction of copper slag are very high with the increase of the content of magnetite in copper slag, and the reaction is hindered resulting in the hard aggregation and growth of iron concentrate [14]. Among these methods, carbothermal reduction process has the advantages of high iron grade and iron recovery ratio. Li et al. [15] utilized coke powder as a reductant to recover iron form copper slag at 1300 ℃, and under the optimized condition, the iron grade and iron recovery ratio were 96.21% and 91.82%, respectively. Renewable resources of reductants have also been investigated, such as cooking oil [16, 17], biochar [18, 19], and diesel oil [20, 21], which are cost-effective and eco-friendly. At temperature above 1200 ℃, it is easy to realize the separation of slag and iron while the smelting reduction takes place, and the additives, such as CaO, CaF_2 and Na_2O, can decrease the reaction temperature [3, 18, 22]. Furthermore, the components of the secondary waste slag after reduction are mainly SiO_2, CaO, Al_2O_3 and MgO, which can be reused as raw materials for the cement and glass ceramics [23, 24].

Due to the advantages of carbothermal reduction reaction of copper slag, more investigations have been focused on this field, including the research of the kinetics of the reduction reaction of copper slag. Zhang et al. [25] found that the controlling step of the reaction between anthracite and copper slag is the diffusion of gas and the activation energy ranges from 61.54 to 146.98 kJ/mol with the variation of reduction rate. Meanwhile, the immersion of reducing agent can compensate for the decrease of reaction temperature, and the reduction rate is about four times faster than the one when the reductant is dispersed on the surface of liquid copper slag [26]. With a floating graphite disk or immersed graphite rod at the temperature from 1250 ℃ to 1450 ℃, the carbothermal reaction of synthetic fayalite slag is controlled by the Boudouard reaction, which is same as the carbothermal reduction of the other iron oxides [27-29], and the activation energy is 246±29 kJ/mol. According to the results of Zhang et al. [30], the coal-based isothermal reduction mechanisms of fayalite with some impurities of magnetite and quartz can be described as two stages: firstly, the phase boundary chemical reaction is the limited step, and the second stage is controlled by diffusion and boundary chemical reaction.

As fayalite is the main iron-bearing component in the copper slag, the reduction kinetics of fayalite is important to investigate the reduction process of copper slag. However, the accuracy of the activation energy of carbothermal reduction of fayalite was affected by the other iron oxides in the fayalite. On the other hand, the investigation methods of the kinetics of carbothermal reduction of fayalite were mainly under the isothermal conditions. It was demonstrated that the variation of heating rate would influence the activation energy and result in the different kinetics parameters even in the same experimental conditions. In fact, strictly isothermal experiments are not possible, as there is always a finite non-isothermal heat-up time (usually a few minutes). Therefore, the pure fayalite and non-isothermal methods were applied in this paper.

The purpose of the present work is to analyze the thermodynamics of carbothermal reduction process of fayalite and precisely investigate the non-isothermal kinetics of reaction between fayalite and graphite at different heating rates. Meanwhile, the activation energy and the kinetic model of the reaction are determined by applying the methods of Flynn-Wall-Ozawa (FWO) [33] and Málek [34], respectively.

2. Thermodynamic analysis of reduction process of fayalite

To confirm the starting temperature of the carbothermal reduction process of fayalite, reduction reaction was analyzed using the FactSage 7.3 software (Version 7.3, GTT-TECHMOLOGIES, Herzogenrath, Germany) based on the Gibbs free energy calculation in the standard state. For the carbothermal reduction of fayalite, the reductants are C and CO generated from the gasification of graphite. The reduction of fayalite with C is called the direct reduction reaction and with CO is called the indirect reaction as shown in Eq. (1) and (2). The Eq. (3) is the gasification of graphite called Boudouard reaction.

$$Fe_2SiO_4(s)+2C(s)=SiO_2(s)+2Fe(s)+2CO(g) \quad (1)$$

$$\Delta G_m^\theta = 346.614 - 0.321T\text{(kJ/mol)}\ (273\text{K}\sim2273\text{K})$$

$$Fe_2SiO_4(s)+2CO(g)=SiO_2(s)+2Fe(s)+2CO_2(g) \quad (2)$$

$$\Delta G_m^\theta = 4.057 + 0.0289T\text{(kJ/mol)}\ (273\text{K}\sim2273\text{K})$$

$$C(s)+CO_2(g)=2CO(g) \quad (3)$$

$$\Delta G_m^\theta = 170.830 - 0.174T\text{(kJ/mol)}\ (273\text{K}\sim2273\text{K})$$

Figure 1 shows the curves of the standard Gibbs free energy change of reactions with variations of the temperature. It can be seen that the starting temperature of direct reduction reaction was 806.79 ℃ in standard state. Because the smelting point of

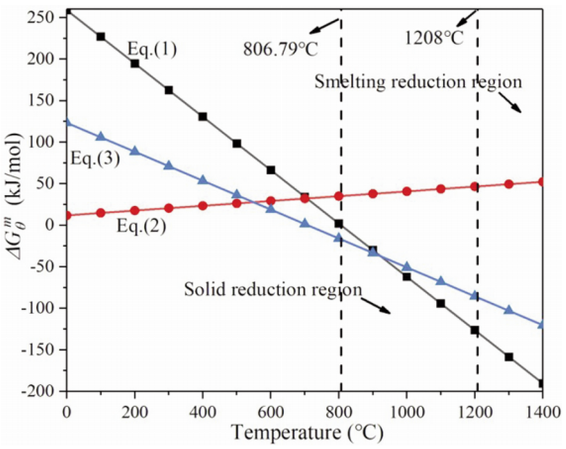

Figure 1. *Standard Gibbs free energy of reactions with variations of temperature*

fayalite is about 1208 °C, the reduction of fayalite can be divided into two regions, i.e., the solid reduction region from 806.79 °C to 1208 °C, which is a solid reduction reaction of fayalite, and smelting redution region from 1208 °C to 1400 °C, where the state of fayalite is liquid. With the increase of temperature, the standard Gibbs free energy of direct reaction (Eq. 1) is increasingly negative, which means that high temperature can promote the direct reduction reaction. From Figure 1, the standard Gibbs free energy of indirect reduction reaction (Eq. 2) became increasingly positive in the range of experimental temperature, indicating that the indirect reduciton reaction could not take place in the standard state.

However, the reduction reactions of fayalite do not always take place in the standard state. Figure 2 shows the relationship between the starting temperature and volume percentage of CO of the direct reduction reaction in the nonstandard state. From Figure 2, it can be evaluated that starting temperature was low in the nonstandard state and it increased when the

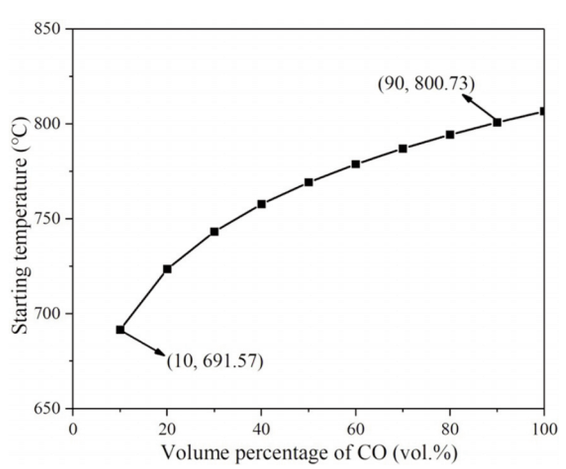

Figure 2. *Relationship between the starting temperature and the content of CO of the direct reduction reaction in the nonstandard state*

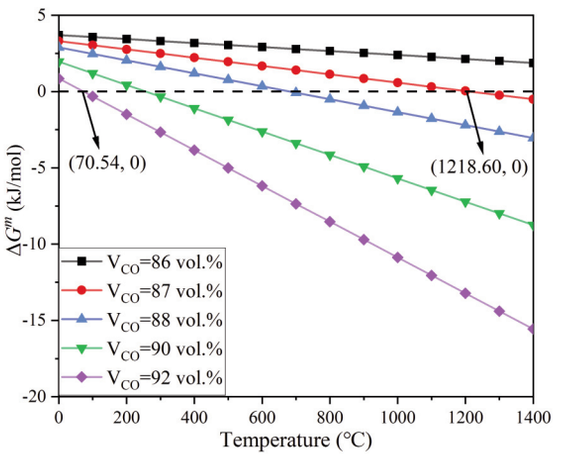

Figure 3. *Gibbs free energy change of the indirect reduction reaction with different content of CO and temperature in the nonstandard state*

content of CO increased in the system. The starting temperature increased to 109.16 °C, while the volume percentage of CO increased from 10 vol.% to 90 vol.%. Figure 3 shows the curves of Gibbs free energy change of the indirect reaction with different content of CO and temperature in the nonstandard state. It can be seen that the content of CO had a significant effect on the indirect reduction. When the volume percentage of CO was 86 vol.%, the values of Gibbs free energy were higher than zero in the range of experimental temperature. With the content of CO increasing, the values of Gibbs free energy became lower gradually, meaning that the indirect reduction reaction of fayalite was possible to take place in the range of experimental temperature. The starting temperature of the indirect reduction of fayalite in the nonstandard state decreased from 1218.60 °C to 70.54 °C, while the volume percentage of CO increased from 87 vol.% to 92 vol.%.

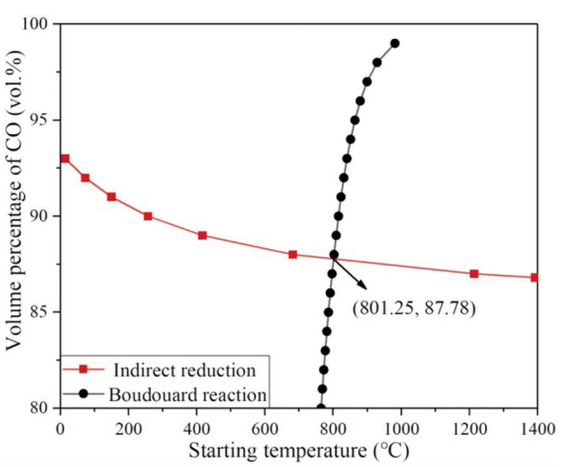

Figure 4. *Relationship between the starting temperature and the content of CO of the indirect reduction reaction and Boundouard reaction in the nonstandard state*

The reductant CO in indirect reduction reaction is generated by the Boudouard reaction as shown in Eq. 3. It can be seen from Figure 4 that the relationship between the starting temperature and the content of CO was the result of the indirect reduction reaction and Boundouard reaction in the nonstandard state. From Figure 4, it can be seen that the 801.25 ℃ was a critical point. While the temperature was higher than 801.25 ℃, there was enough CO generated by Boudouard reaction to make the indirect reduction reaction takes place. In other words, the direct reduction reaction occurred below 801.25 ℃. With the increasing of temperature, the content of CO required for the indirect reduction reaction decreased.

3. Materials and methods

The raw materials, fayalite (Alfa Aesar, 96 wt%) and graphite (Macklin, 99.99 wt%), were ground to make more than 80 wt% of samples pass through the sieve of 0.075 mm, respectively. Thermogravimetric analyzer (STA449C, NETZSCH, Germany) was used to conduct the non-isothermal carbothermal reduction reaction under high pure argon atmosphere at 50 mL/min. For each experiment, approximately 10~15 mg mixtures were heated from ambient temperature to 1400 ℃ in corundum crucible (D: 6.5 mm, H: 2.0 mm). Firstly, the content of graphite in each batch was investigated from ambient temperature to 1400 ℃ at 10 ℃/min for making the fayalite reduced sufficiently. According to the Eq. (1), when the value of C/O was 1.0, the carbon content was 0.58g/g fayalite. The value of C/O of 1.0 meant that the graphite content was enough to make all fayalite reduced exactly. Then, the carbothermal reduction of fayalite with same content of graphite was carried on in different heating ratio, 2.5, 5, 10, and 20 ℃/min, respectively, to calculate the activation energy and study the reaction model.

4. Results and discussion

4.1. TG results

Figure 5 depicts the mass loss of the sample at different carbon content from ambient temperature to 1400 ℃. The values of C/O were from 1.0 to 2.2. According to the mass loss in Figure 5, the reduction rate of the reaction (α) could be calculated by the following equation:

$$\alpha = \frac{m_0 - m_t}{m_0 - m_T} \times 100\% \quad (4)$$

where m_0, m_t and m_T represent the initial sample mass, the sample mass at reaction time t, and the final sample mass, respectively.

Figure 6 shows the reduction rate of carbothermal

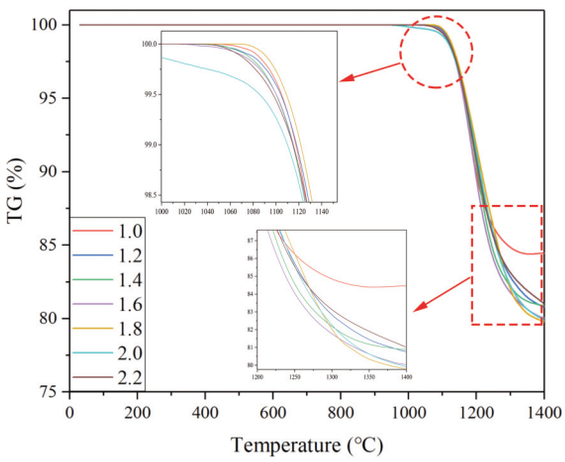

Figure 5. *Mass loss at different carbon content*

reduction of fayalite at different carbon content from ambient temperature to 1400 ℃. The reduction rate increased obviously from about 1100 ℃ to about 1300 ℃ and then increased slowly with the increased temperature. The highest reduction rate was 90.70% while the value of C/O was 2.0. The starting temperature of reduction reaction of fayalite was about 950 ℃. The reduction rate increased resulting from that the kinetic condition of reaction could be improved with the increase of carbon content. However, excessive carbon content increased the viscosity and limited the mass transfer. According to the results of different carbon content, the value of C/O of 2.0 was chosen to calculate the activation energy and investigate the reaction model.

Figure 7 presents the curves of mass loss (TG) of sample with value of C/O of 2.0 from ambient temperature to 1400 ℃ at different heating rates. It can be seen from Figure 7 that at the temperature below 1100 ℃, the mass decreased slightly, and then, the mass loss became sharp with the increase of temperature. Finally, the tendency of mass loss leveled off from about 1200 ℃ to 1400 ℃. According

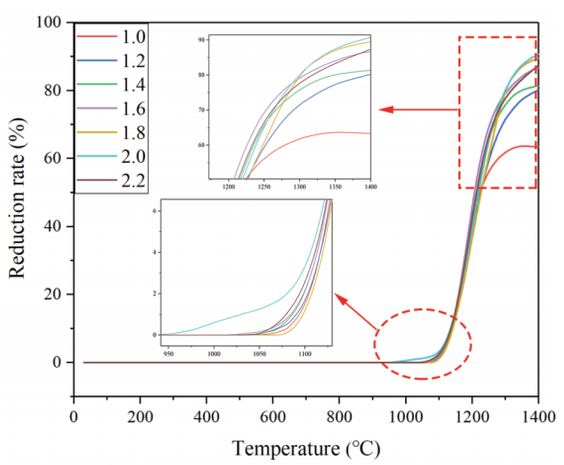

Figure 6. *Reaction rate at different carbon content*

to the thermodynamic analysis, the indirect reduction reaction took place until 801.25 ℃ in the nonstandard state. However, the content of CO was not enough to make the indirect reduction reaction take place while the temperature was lower than 1100 ℃. On the contrary, the volatilization of impurities in fayalite and graphite and the direct reduction reaction influenced the slight loss of mass. When the temperature was higher than 1100 ℃, the enough CO provided by Boundouard reaction promoted the indirect reduction reaction of fayalite, making the mass decrease obviously. With the consumption of reactants, the mass loss leveled off until the end. Although the tendencies of the TG curves were similar at different heating rates in Figure 7, the slower heating rate made the reaction more complete and it started at a lower temperature. When the heating rate was 2.5 ℃/min, the reaction took place at about 827.61 ℃ and the reaction finished at about 1334.43 ℃, where the value of mass loss was 77.84 wt%. When the heating rate was 20 ℃/min, the reaction occurred at about 943.30 ℃ and the reaction finished at about 1398.73 ℃, where the value of mass loss was 79.92 wt%.

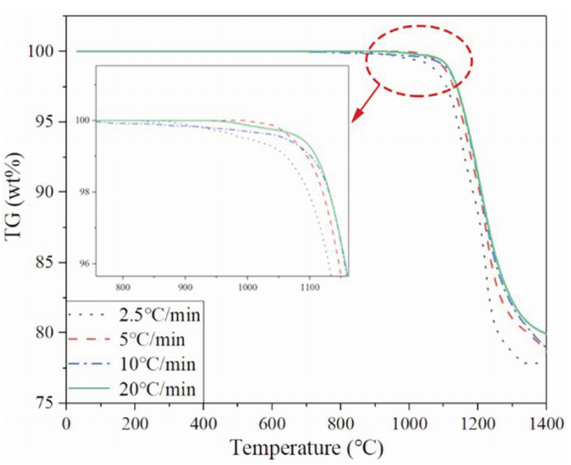

Figure 7. *Mass loss (TG) at different heating rates*

Figure 8 shows the variation of reduction rates at different heating rates. The largest and smallest reduction rates were 99.10% at 2.5 ℃/min, and 90.70% at 20 ℃/min, respectively. Therefore, the reduction rate at slower heating rate was higher than the one at faster heating rate at the same temperature, meaning that the content of reactants at slower heating rate was higher.

The reduction rate can be calculated according to the derivative of the reduction rate in Figure 8 with respect to time. Considering the temperature has the linear relationship with time, Figure 9 shows the reaction rates of carbothermal reduction of fayalite against the temperature at different heating rates. It can be indicated that the temperature at largest

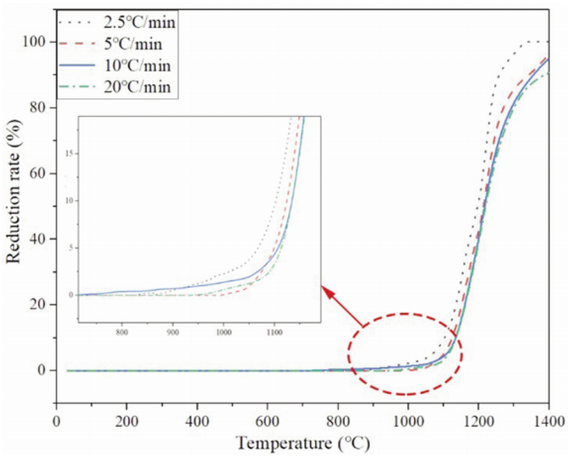

Figure 8. *Variation of reduction rate at different heating rates*

reaction rate decreased with the increase of heating rate, which was 1222 ℃, 1224 ℃, 1216 ℃, and 1207 ℃, respectively. Furthermore, the maximum value of reaction rate increased from 2.3 %/min at 2.5 ℃/min to 11.2 %/min at 20 ℃/min. The results consisted with the results in Figure 6. The contents and activities of reactants at faster heating rate were higher at the same temperature, making the reaction rate higher. The reaction rate exhibited a decreasing tendency when the reaction temperature was higher than 1200 ℃. That occurred due to the fact that the indirect reaction between fayalite and CO was sharp, and consumed a

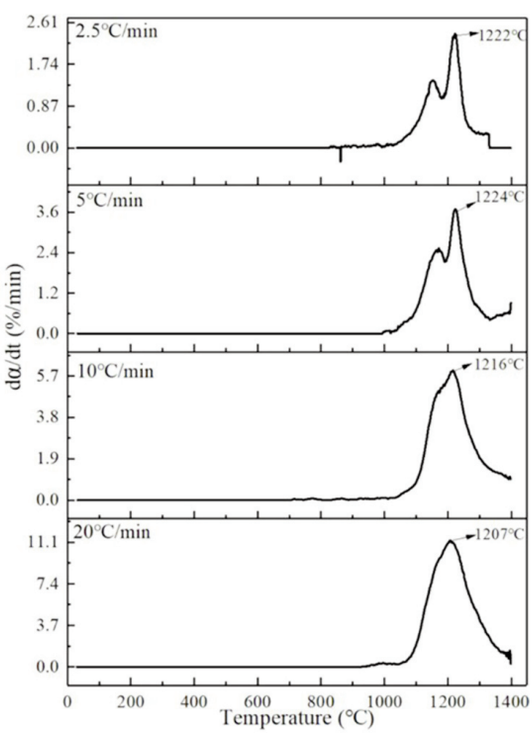

Figure 9. *Reaction rate of carbothermal reduction of fayalite at different heating rates*

large number of reactants, resulting in the decrease of the activities of reactants and reaction rate.

4.2. Models of kinetic calculation

The FWO model was used to calculate the carbothermic reduction reaction activation energy of fayalite, and the expression is shown as follows:

$$\lg\beta = \lg[\frac{AE}{RG(\alpha)}] - 2.315 - 0.4567\times\frac{E}{RT} \quad (5)$$

where β, A, E, R, and T represent the heating rate ($K\cdot min^{-1}$), the preexponential factor (s^{-1}), the activation energy ($J\cdot mol^{-1}$), the gas mole constant (8.314 $J\cdot(mol\cdot K)^{-1}$) and the absolute temperature (K), respectively. $G(\alpha)$ represents an integral form of the reaction model.

According to the Eq. 5, the value of E can be obtained from the slope of lgβ versus $1/T$.

The Málek model is applied to determine the reaction model, and the expression is shown as follows:

$$y(\alpha) = G(\alpha)f(\alpha)/G(0.5)f(0.5) \quad (6)$$

$$y(\alpha) = (\frac{T}{T_{0.5}})^2(\frac{d\alpha}{dt})\Big/(\frac{d\alpha}{dt})_{0.5} \quad (7)$$

where $f(\alpha)$ represents a differential form of the reaction model, $G(0.5)$, $f(0.5)$, $T0.5$ and $(d\alpha/dt)_{0.5}$ are the values of integral equation, differential equation, temperature and reaction rate corresponding to the reduction rate α=0.5, respectively.

The general solid reaction models list is shown in Table 1. According to the method of Málek model, the standard curves of $y(\alpha)$ against α can be depicted using the models in Table 1. Then, the plots of experimental data of $y(\alpha)$ can be calculated by the Eq. (7). Finally, the reaction models can be obtained through comparing the standard curves and the plots of experimental data.

4.3. Calculation and discussion of kinetic parameters

According to the FWO model shown in Eq. 5, Figure 10 shows the plots of logarithm of heating rate (lgβ) vs. reciprocal temperature ($1/T$), indicating the logarithm of heating rate had a good linear relationship with reciprocal of temperature. Based on the slope of the fitted lines, the calculated values of activation energy for carbothermic reduction of

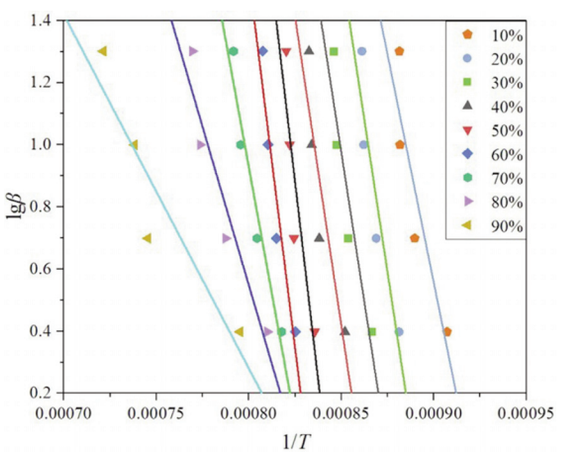

Figure 10. *Plots of logarithm of heating rate (lgβ) vs reciprocal temperature (1/T) [36]*

Table 1. *General models of solid reactions [30, 34, 35]*

No.	Differential Equation $f(\alpha)$	Integral Equation $G(\alpha)$	Models
1	$1-\alpha$	$-\ln(1-\alpha)$	One-dimension random nucleation
2	$(1-\alpha)^{3/2}$	$2[(1-\alpha)^{-1/2}-1]$	Chemical reaction (n=1.5)
3	$(1-\alpha)^2$	$(1-\alpha)^{-1}-1$	Chemical reaction (n=2)
4	1	α	One-dimension phase boundary-controlled reaction
5	$2(1-\alpha)^{1/2}$	$1-(1-\alpha)^{1/2}$	Two-dimension phase boundary-controlled reaction
6	$3(1-\alpha)^{2/3}$	$1-(1-\alpha)^{1/3}$	Three-dimension phase boundary-controlled reaction
7	α	$\ln\alpha$	One-dimension nucleation-uniform growth
8	$1/2\alpha$	α^2	One-dimension diffusion
9	$-1/[\ln(1-\alpha)]$	$(1-\alpha)\ln(1-\alpha)+\alpha$	Two-dimension diffusion
10	$3/2[(1-\alpha)^{-1/3}-1]$	$1-2\alpha/3-(1-\alpha)^{2/3}$	Three-dimension diffusion (Jander Equation)
11	$3/2(1-\alpha)^{2/3}[1-(1-\alpha)^{1/3}]$	$[1-(1-\alpha)^{1/3}]^2$	Three-dimension diffusion

fayalite are shown in Figure 10. It should be noted that only the TG results corresponding to the reduction rate of reaction ranging from 10% to 90% were used, taking in consideration that the calculating deviation was easy to introduced at beginning and end of the reaction processes [30].

From Figure 11, it can be seen that the activation energy first increased as the reaction proceeded and then decreased when the reduction rate of reaction was higher than 50%. The largest value of activation energy was 928.35 kJ/mol, which corresponded to the reduction rate α=50%. In the initial stage, the increasing of the activation energy was attributed to the direct reduction between fayalite and graphite. Under this condition, the poor kinetics condition between solid-solid reactions restricted the diffusion of materials in the reaction. With the reaction temperature increasing, fayalite was easier to make phase transition, and most of fayalite decomposed into iron oxides and silicon [35]. Meanwhile, the gasification of graphite provided CO to help the indirect reduction between fayalite and CO proceeded at a larger reaction rate. Both of those accelerated the reaction process and the activation energy decreased.

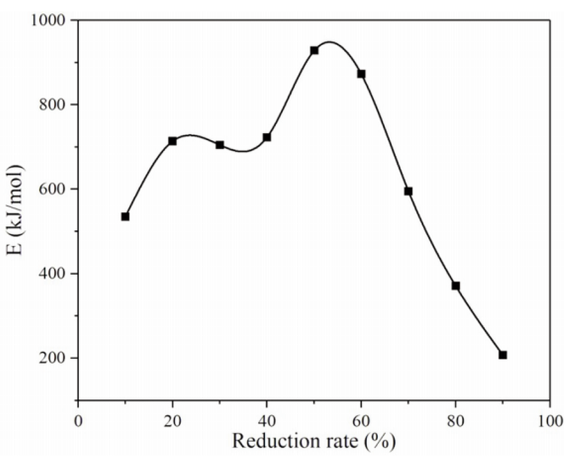

Figure 11. *Activation energy as a function of extent of reaction [36]*

Meanwhile, it was also found from Fig.11 that the average carbothermal reduction reaction activation energy of fayalite was 527.41 kJ/mol. The results of the present study and the reported activation energy of carbothermal reduction of fayalite by other researchers are exhibited in Table 2 for comparison. The activation energy of the carbothermal reduction of fayalite in present study was higher than those reported in previous studies. The activation energy depends on many factors, such as input material, gas composition and temperature scheme of experiment. The difference of activation energy in present study was mainly attributed to the factor that the reactant in previous investigations was synthetic fayalite or copper slag, which may have cointained impurities (such as other iron oxides), and that made the reduction reaction easier. Therefore, the values of activation energy of reduction reaction were lower than that in the current study. Furthermore, for the isothermal experiment process, the reduction occurred during the heating process, making the activation energy of the carbothermal reduction of fayalite decrease.

Table 2. *Activation energy of carbothermal reduction of fayalite in the present work and literatures*

Sources	Samples	Temperature (°C)	Activation energy (kJ/mol)
Zhang et al. [25]	Fayalite from copper slag	Isothermal kinetics: 1000-1200	118.1
Warczok et al. [27]	Synthetic fayalite	Isothermal kinetics: 1250-1450	246.0
Zhang et al. [30]	Fayalite powder obtained from copper slag and coal	Isothermal kinetics: 850-1000	185.07-225.67
Lin et al. [37]	Fayalite from copper slag	Isothermal kinetics: 1000-1200	373.6
Present work	Pure fayalite	Non-isothermal kinetics: 30 to 1400	527.4

To analyze the reaction model of reduction reaction of fayalite accurately, the standard curves are depicted in Figure 12. The numbers in Figure 12 corresponded to the reaction models in Table 1. It can be seen from Fig. 12 that there is no model that fits the whole reaction process. When the reduction rate was lower than 50%, the reduction of fayalite could be expressed by secondary chemical reaction model (No. 3) with the integral form of $(1-\alpha)^2$, and subsequently by one-dimensional nucleation and uniform growth (No. 7) with the integral form of $\ln\alpha$ [36]. At the beginning of the carbothermal reduction of fayalite, there was not enough CO to be provided to make the reduction reaction proceed sharply. Therefore, the chemical reaction of gasification of graphite was the controlling step of the carbothermal reduction of fayalite, which was consistent with the results

reported by other researchers [29]. In other words, the kinetics of the carbothermal of fayalite can be improved by increasing the reaction rate constant of the gasification of graphite and the special surface area of the graphite in the low reduction rate [38]. As the reaction proceeded, the generated CO provided a good kinetics condition for the carbothermal reduction of fayalite, and the controlling step of the reaction was the nucleation and growth of the metallic iron.

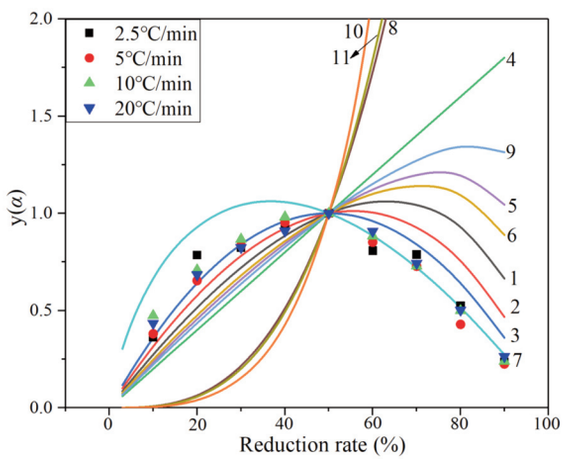

Figure 12. *Standard curves of the plots of y(α) against α and experimental data [36]*

5. Conclusions

1) In nonstandard state, the starting temperature of direct reduction increased with the increase of content of CO. While the volume percentage of CO was higher than 86 vol.%, the indirect reduction occurred in the range of experimental temperature. Meanwhile, Boudouard reaction promoted the indirect reduction that took place when the temperature was higher than 801.25 ℃.

2) At the temperature below 1100 ℃, the main reduction reaction was the reaction between fayalite and graphite. With the temperature increase, the fayalite reacted with CO generated from the gasification of graphite, which had a good reaction kinetic conditions and made the reaction proceed at a faster rate.

3) The activation energy of carbothermal reduction of fayalite increased with the increase of reduction rate firstly and then decreased when the reduction rate was higher than 50%. The average activation energy was 527.41 kJ/mol. The carbothermal reduction of fayalite was multistep reaction. The controlling step of the carbothermal reduction in the initial stage was the gasification of graphite, where there was no enough CO to make the reduction reaction proceed sharply. As the reaction proceeded, the generated CO provided a good kinetics condition for the carbothermal reduction of fayalite, and the controlling step of the reaction was the nucleation and growth of the metallic iron.

Acknowledgments

This work was supported by Joint Research Fund of National Natural Science Foundation-China BaoWu Steel Group Co., Ltd (No. U1960108) and Hubei Provincial Special Project on Technology Innovation (Foreign Scientific and Technological Cooperation) (No. 2017AHB042). Meanwhile, the authors will acknowledge that this paper was partly presented at 11th International Symposium on High-Temperature Metallurgical Processing, in The Minerals, Metals & Materials Series, and is published with the permission of the Springer, Cham.

Author's contributions

G.-J. Ma, Z. Li,: conceptualization, Z. Li, G.-J. Ma, J.-J. Zou, D.-L, Zheng, X. Zhang: experiment, test and validation; Z. Li:, writing-original draft.

Data availability

The data of this study could be obtained by contacting with the corresponding author via e-mail.

Conflict of Interest

The authors state that there is no conflict of interest.

References

[1] D. Orac, M.Laubertova, J. Piroskova, D.Klein, R. Bures, J. Klimko, Characterization of dusts from secondary copper production, Journal of Mining and Metallurgy, Section B: Metallurgy, 56(2) (2020) 221-228. https://doi.org/10.2298/JMMB190820011O

[2] W.G. Davenport, M. King, M. Schlesinger, A.K. Biswas, C.J. Yang, F. Dong, Extractive Metallurgy of Copper, 4th ed., Chemical Industry Press, Beijing, (2006), 20.

[3] X.Y. Meng, Y. Li, H.Y. Wang, Y.D. Yang, A. Mclean, Effects of Na2O additions to copper slag on iron recovery and the generation of ceramics from the non-magnetic residue, Journal of Hazardous Materials, 339(15) (2020) 122845. https://doi.org/10.1016/j.jhazmat.2020.122845

[4] Y. Feng, J. Kero, Q.X. Yang, Q.S. Chen, F. Engström, C. Samuelsson, C.C. Qi, Mechanical activation of granulated copper slag and its influence on hydration heat and compressive strength of blended cement, Materials, 12(5) (2019) 772. https://doi.org/10.3390/ma12050772

[5] D.B. Zhang, Y. Zhang, T. Cheng, Measurement of grass root reinforcement for copper slag mixed soil using

improved shear test apparatus and calculating formulas, Measurement, 118 (2018) 14-22. https://doi.org/10.1016/j.measurement.2018.01. 005

[6] J.P. Wang, U. Erdenebold, A study on reduction of copper smelting slag by carbon for recycling into metal values and cement raw material, Sustainability-Basel, 12(4) (2020) 1421. https://doi.org/10.3390/su12041421

[7] J.H. Chen, W.J. Mi, H.Y. Chen, B. Li, K.C. Chou, X.M. Hou, Iron oxide recovery from fayalite in water vapor at high temperature, Journal of Mining and Metallurgy, Section B: Metallurgy, 54(1) B (2018) 1-8. https://doi.org/10.2298/JMMB160926011C

[8] D.Q. Zhu, J.W. Xu, Z.Q. Guo, J. Pan, S.W. Li, L.T. Pan, C.C. Yang, Synergetic utilization of copper slag and ferruginous manganese ore via co-reduction followed by magnetic separation process, Journal of Cleaner Production, 250(20) (2020) 119462. https://doi.org/10.1016/j.jclepro.2019.119462

[9] H. Han, D. Duan, P. Yuan, S. Chen, Recovery of metallic iron from high phosphorus oolitic hematite by carbothermic reduction and magnetic separation Ironmaking & Steelmaking, 42(7) (2015) 542-547. https://doi.org/10.1179/1743281214Y.0000000259

[10] W. Han, Q.W. Qin, Recovery of copper and iron from copper slag, Mining and metallurgy, 18(2) (2009) 9-12. (in Chinese)

[11] P.G. Jiang, J.S. Liu, Y.Y. Xiao, X.H. Tan, W.J. Liu, Recovery of iron from copper slag via modified roasting in CO-CO2 mixed gas and magnetic separation, Journal of Iron and Steel Research International, 27(2020) 796-806. https://doi.org/10.1007/s42243-020-00413-0

[12] Q.J. Li, F.X. Yang, Z.Y. Wang and S.Y. Liu, Study on Mechanism of Oxidation Modification of Copper Slag, Transactions of the Indian Institute of Metals, 72 (2019) 3223-3231. https://doi.org/10.1007/s12666-019-01788-9

[13] B.F. Zhan, Z.L. Huang, N. Yang, Y.F. Liu, C.P. Jiao, Recovery of iron from copper-slag with process of roasting-leaching-magnetic separation, Mining and metallurgical engineering, 35(2) (2015) 103-106. (in Chinese)

[14] J. Palacios, M. Sánchez, Wastes as resources: update on recovery of valuable metals from copper slags, Mineral Processing and Extractive Metallurgy, 120(4) (2011) 218-223. https://doi.org/10.1179/1743285511Y.0000000020

[15] K.Q. Li, S. Ping, H.Y. Wang, W. Ni, Recovery of iron from copper slag by deep reduction and magnetic beneficiation, International Journal of Minerals, Metallurgy, and Materials, 20 (2013) 1035-1041. https://doi.org/10.1007/s12613-013-0831-3

[16] B. Li, X.B. Wang, H. Wang, Y.G. Wei, J.H. Hu, Smelting reduction and kinetics analysis of magnetic iron in copper slag using waste cooking oil, Scientific Reports, 7 (2017) 2406. https://doi.org/10.1038/s41598-017-02696-y

[17] S.W. Zhou, Y.G. Wei, S.Y. Zhang, B. Li, H. Wang, Y.D. Yang, M. Barati, Reduction of copper smelting slag using waste cooking oil, Journal of Cleaner Production, 236(1) (2019) 117668. https://doi.org/10.1016/j.jclepro.2019.117668

[18] Z.L. Zuo, Q.B. Yu, S.Y. Luo, J.K. Zhang, E. Zhou, Effects of CaO on two-step reduction characteristics of cpper slag using biochar as reducer: thermodynamic and kinetics, Energty & Fuels, 34(1) (2020) 491-500. https://doi.org/10.1021/acs.energyfuels.9b03274

[19] Z.L. Zuo, Q.B. Yu, H.Q. Xie, F. Yang, Z.C. Han, Q. Qin, Direct reduction of copper slag-carbon composite pellets by coal and biochar, Environmental Technology, 41(17) (2020) 2240-2252. https://doi.org/10.1080/09593330.2018.1561757

[20] C. Wang, M. Zheng, D.F. Zhu, X.Q. Feng, Reduction of Fe3O4 in copper slag by diesel oil in the presence of nitrogen, Chemical Industry and Engineering Process, 33(5) (2014) 33:1101-1107. (in Chinese)

[21] B. Li, Y.G. Wei, H. Wang, Y.D. Yang, Reduction of magnetite from copper smelting slag using petro-diesel and biodiesel, ISIJ International, 58(6) (2018) 1168. http://dx.doi.org/10.2355/isijinternational.ISIJINT-2017-723

[22] Z.Y. Yang, Z.H. Ma, The effect of basicity and calcium fluoride on glass-ceramic production and iron recovery from copper slag, Steel Research International, 83(3) (2017) 1600145. https://doi.org/10.1002/srin.201600145

[23] P. Sarfo, G. Wyss, G.J. Ma, A. Das, C. Young, Carbothermal reduction of copper smelter slag for recycling into pig iron and glass, Mineral Engineering, 107 (2017) 8-19. https://doi.org/10.1016/j.mineng.2017.02.006

[24] Z.H. Yang, Q. Lin, J.X. Xia, Y. He, G.D. Liao, Y. Ke, Preparation and crystallization of glass–ceramics derived from iron-rich copper slag, Journal of Alloy and Compounds, 574 (15) (2013) 354-360. https://doi.org/10.1016/j.jallcom.2013.05.091

[25] H. Zhang, G. Wang, S.H. Zhang, J.S. Wang, Q.G. Xue, Direct reduction kinetics of copper slag, Nonferrous Metals Science and Engineering, 10(1) (2019) 28-33. (in Chinese)

[26] A. Mitrašinović, Effect of temperature and graphite immersion method on carbothermic reduction of fayalite slag, JOM, 69 (2017), 1682-1687. https://doi.org/10.1007/s11837-017-2455-y

[27] A. Warczok, T.A. Utigard, Fayalite slag reduction by solid graphite, Canadian Metallurgical Quarterly, 37(1) (1998) 27-39. https://doi.org/10.1016/S0008-4433(97)00034-7

[28] Y.Y. Zhang, W. Lv, X.W. Lv, S.P. Li, C.G. Bai, B. Song, K.X. Han, Isothermal reduction kinetics of Panzhihua ilmenite concentrate under 30vol% CO-70vol% N2 atmosphere, International Journal of Minerals, Metallurgy, and Materials, 24 (2017) 240-248. https://doi.org/10.1007/s12613-017-1401-x

[29] C.Y. Ding, X.W. Lv, S.W. Xuan, K. Tang, C.G. Bai, Crystallization kinetics of 2CaO center dot Fe2O3 and CaO center dot Fe2O3 in the CaO-Fe2O3 system, ISIJ International, 56(7) (2016) 2118-2125. https://doi.org/10.2355/isijinternational

[30] L. Zhang, Y. Zhu, W.Z. Yin, B. Guo, F. Rao, J.G. Ku, Isothermal coal-based reduction kinetics of fayalite in copper slag, ACS Omega, 5(15) (2020) 8605-8612. https://doi.org/10.1021/acsomega.9b04497

[31] S. Vyazovkin, A.K. Burnham, J.M. Criado, L.A. Pérez-Maqueda, C. Popescu, N. Sbirrazzuoli, ICTAC kinetics committee recommendations for performing kinetic computations on thermal analysis data, Thermochim. Acta, 520(1-2) (2011) 1-19. https://doi.org/10.1016/j.tca.2011.03.034

[32] G.J. Cheng, J.X. Liu, Z.C. Liu, M.S. Chu, X.X. Xue, Non-isothermal reduction mechanism and kinetics of

high chromium vanadium–titanium magnetite pellets, Ironmaking & Steelmaking, 42(1) (2015), 17-26. https://doi.org/10.1179/1743281214Y.0000000193

[33] T. Ozawa, A new method of analyzing thermogravimetric data, Bulletin of the Chemical Society of Japan, 38(1965) 1881-1886. http://doi.org/10.1246/bcsj.38.1881

[34] J. Málek, A computer program for kinetic analysis of non-isothermal thermoanalytical data, Thermochim. Acta, 138(2) (1989) 337-346. http://doi.org/10.1016/0040-6031(89)87270-3.

[35] S.Y. Luo, J.Y. Zhang and T.P. Zhou: Materials Reports, 14(2000) 6-7, 40. (in Chinese)

[36] Z. Li, G.J. Ma, X. Zhang, W. Zhang, 11th International Symposium on High-Temperature Metallurgical Processing, The Minerals, Metals and Materials 2020, pp: 295-302.

[37] Q. Lin, Master thesis, Chongqing University (2017). (accessed 2020-08-30) (in Chinese)

[38] X.G. Huang, Iron and Steel Metallurgical Principles, 4th ed, Metallurgical Industrial Press, Beijing, (2013), 132-144. (in Chinese)

KARBOTERMIČKA REDUKCIJA FAJALITA: TERMODINAMIČKA I NEIZOTERMSKA KINETIČKA ANALIZA

Z. Li [a, b], G.-J. Ma [a, b, *], J.-J. Zou [a, b], D.-L, Zheng [a, b], X. Zhang [a, b]

[a] Glavna državna laboratorija za refraktorne materijale i metalurgiju, Univerzitet za nauku i tehnologiju u Vuhanu, Vuhan, Kina

[b] Glavna laboratorija za crnu metalurgiju i iskorišćenje resursa pri Ministarstvu obrazovanja, Univerzitet za nauku i tehnologiju u Vuhanu, Vuhan, Kina

Apstrakt

U ovom radu je ispitana termodinamika i kinetika karbotermičke redukcije fajalita neizotermskom metodom u kombinaciji sa termogravimetrijskim analizatorom i primenom Ozawa-Flynn-Wall (OFW) i Malekovog modela. Termodinamička analiza je pokazala da je početna temperatura reakcije direktne redukcije fajalita bila 806,79 °C u standardnom stanju. Reakcija indirektne redukcije nije mogla da se odvija u standardnom stanju. Kada je zapreminski procenat CO bio veći od 86 vol.% u nestandardnom stanju, indirektna redukcija je bila moguća u opsegu temperature eksperimenta. Buduarova reakcija je takođe mogla da podstakne proces indirektne redukcije. Rezultati kinetičke analize su pokazali da je na temperaturi manjoj od 1100 °C glavna reakcija redukcije bila direktna redukcija fajalita i grafita. Sa povećanjem temperature fajalit je reagovao sa CO koji je nastao tokom gasifikacije grafita. Kada se brzina redukcije povećala sa 0% na 50%, energija aktivacije se povećala na 524,41 kJ/mol. Nakon toga je energija aktivacije opadala sa povećanjem brzine redukcije. Karbotermička redukcija fajalita se odvijala u više koraka. Kontrolni korak u početnoj fazi je bila gasifikacija grafita. Kako se reakcija odvijala, generisani CO je obezbedio dobar kinetički uslov za karbotermičku redukciju fajalita, a kontrolni korak reakcije je bila nukleacija i povećanje količine metalnog gvožđa.

Ključne reči: *Karbotermalna redukcija fajalita; Termodinamika; Neizotermska kinetika*